Observation of Caroli–de Gennes–Matricon Vortex States in $YBa_2Cu_3O_{7-\delta}$

Berthod, Christophe; Maggio-Aprile, Ivan; Bruer, Jens Erik; Erb, Andréas; Renner, Christoph

How to cite

BERTHOD, Christophe et al. Observation of Caroli–de Gennes–Matricon Vortex States in $YBa_2Cu_3O_{7-\delta}$. In: Physical Review Letters, 2017, vol. 119, n° 23, p. 237001. doi: 10.1103/PhysRevLett.119.237001

This publication URL: https://archive-ouverte.unige.ch/unige:99962
Publication DOI: 10.1103/PhysRevLett.119.237001

Observation of Caroli–de Gennes–Matricon Vortex States in $YBa_2Cu_3O_{7-\delta}$

Christophe Berthod,[1] Ivan Maggio-Aprile,[1] Jens Bruér,[1] Andreas Erb,[2] and Christoph Renner[1,*]
[1]*Department of Quantum Matter Physics, University of Geneva, 24 quai Ernest-Ansermet, 1211 Geneva, Switzerland*
[2]*Walther-Meissner-Institut, Bayerische Akademie der Wissenschaften, Walther-Meissner-Strasse 8, D-85748 Garching, Germany*
(Received 19 June 2017; revised manuscript received 19 September 2017; published 4 December 2017)

The copper oxides present the highest superconducting temperature and properties at odds with other compounds, suggestive of a fundamentally different superconductivity. In particular, the Abrikosov vortices fail to exhibit localized states expected and observed in all clean superconductors. We have explored the possibility that the elusive vortex-core signatures are actually present but weak. Combining local tunneling measurements with large-scale theoretical modeling, we positively identify the vortex states in $YBa_2Cu_3O_{7-\delta}$. We explain their spectrum and the observed variations thereof from one vortex to the next by considering the effects of nearby vortices and disorder in the vortex lattice. We argue that the superconductivity of copper oxides is conventional, but the spectroscopic signature does not look so because the superconducting carriers are a minority.

DOI: 10.1103/PhysRevLett.119.237001

Type-II superconductors immersed in a magnetic field let quantized flux tubes perforate them: the Abrikosov vortices. This remarkable property underlies and often limits many applications of superconductors. In 1964, Caroli, de Gennes, and Matricon used the Bardeen-Cooper-Schrieffer (BCS) theory of superconductivity to predict that vortices in type-II superconductors host a collection of localized electrons bound to their cores [1]. The direct observation of these localized states 25 years later by scanning tunneling spectroscopy (STS) is a spectacular verification of the BCS theory [2]. The formation of vortex-core bound states is an immediate consequence of the superconducting condensate being composed of electron pairs, while excitations in the vortex, being unpaired, have a different topology. Core states are, therefore, a robust property of superconductors, like edge states in topological insulators, irrespective of the origin and symmetry of the force that glues the electrons into pairs. In spectroscopy, they appear in the clean limit $\ell \gg \xi$ as a zero-bias peak in the local density of states (LDOS) at the vortex center, where ℓ and ξ are the electron mean free path and superconducting coherence length, respectively, or as a structureless LDOS in the dirty limit $\ell \lesssim \xi$ [3]. Next to $NbSe_2$ [2,4], the core states were seen by STS in several superconducting materials [5–10], including the pnictides, which are believed to host unconventional pairing [11–15]. The high-T_c cuprates stand out as the only materials in which the vortex-core states have been looked for but not found. In $YBa_2Cu_3O_{7-\delta}$ (Y123), discrete finite-energy structures initially believed to be vortex states [16,17] were recently shown to be unrelated to vortices [18]. In $Bi_2Sr_2CaCu_2O_{8+\delta}$ (Bi2212), the vortex cores present no trace of a robust zero-bias peak, but instead very weak finite-energy features apparently related to a charge-density wave order [19–24].

The absence of vortex states in cuprates is challenging the existing theories. Because these states are topological they are robust [25,26], and they survive modifications of the BCS theory like strong-coupling extensions [27] that do not change the nature of the condensate. To explain the cuprate vortex phenomenology, one needs either to leave BCS theory [28–32] or to extend it by including additional order parameters that condense inside the vortex cores and gap out the zero-bias peak [33–35]. To date, none of these approaches has given a satisfactory account of the phenomenology observed by STS. The discovery that the low-energy structures in Y123 do not belong to vortices [18] suggests that these theoretical efforts have been misguided.

The electronic structure of the cuprate high-T_c superconductors (HTS) is notoriously complex, as manifested in a rich phase diagram. This complexity reveals a competition of different effective interactions, from which a variety of individual and collective modes emerges progressively as the temperature is lowered towards the ground state in which the system freezes at absolute zero, and which continues to keep the secret of the most stable superconductivity ever observed. It is generally believed that the phenomena taking place close to the Fermi surface—charge, spin, pairing orders, and their fluctuations—all derive from a single band [36] or a small subset of bands [37] in the CuO_2 layer(s). Consistently, the interpretations of STS spectra [38] have postulated that all electrons contributing to the measured LDOS are excited out of the superconducting condensate, in agreement with Leggett's theorem [39]. On the other hand, it is well known that for all cuprates, at any doping, the superfluid density remains much smaller than the electron density [40–42]. Our recent high-resolution STS experiments on Y123 have also revealed that only a fraction of the signal recorded on the sample surface is of superconducting origin [18]. Early

specific-heat measurements have given a similar hint [43]. We are therefore lead to a new paradigm, in which the low-energy electronic state of the HTS involves a minority superconducting channel in parallel with nonsuperconducting majority charges guilty for the pseudogap and the associated orders. Here we show that the minority carriers are fairly conventional in the superconducting state, showing Caroli–de Gennes–Matricon states in the vortex cores as predicted by the BCS theory for d-wave superconductors.

STS measurements with a normal metal tip do not discriminate the superconducting (SC) and nonsuperconducting (NSC) channels and collect electrons from each. Our working hypothesis is that the tunneling conductances originating from the SC and NSC channels are additive. An earlier report in which vortex-induced changes were tracked in Bi2212 rested on a different scenario, namely, the vortices would suppress locally the condensate and reveal a competing magnetic order [44]. As the NSC is not known, a simple subtraction to reveal the SC is not feasible. Yet, inhomogeneities of the SC like those induced by vortices can be singled out by subtracting the tunneling conductance outside vortices from that inside. If the formation of a vortex leaves the NSC unchanged, this procedure eliminates the NSC and permits a comparison of the SC inhomogeneities with the BCS theory. Figure 1(a) shows the LDOS predicted by the BCS theory at and near the center of an isolated vortex in a two-dimensional superconductor with electronic structure similar to that of Y123 [45]. The prominent feature is the zero-energy peak localized at the core center. With increasing distance from the core, the peak is suppressed with or without a splitting depending on the direction. Note that this LDOS anisotropy is unrelated to the d-wave gap anisotropy. In the quantum regime $k_F\xi \sim 1$ relevant for Y123, the vortex size is comparable with the Fermi wavelength and the Fermi-surface anisotropy determines the vortex structure [52,53]. In the Supplemental Material, Fig. S8 [45] indeed shows that the zero-bias LDOS is locked to the crystal rather than gap-node directions. For a meaningful comparison with experiment, the LDOS far from the vortex must be subtracted, as done in Fig. 1(b).

Figure 2(a) shows a 90×90 nm^2 area on the surface of Y123, where 19 inhomogeneities can be identified as vortex cores. Details about the sample preparation and measurement technique were reported in Ref. [18]. Because of the large NSC, the contrast due to vortices is weak; it is maximized by mapping the ratio of the STS tunneling conductance at 5 and 17 mV bias [Fig. 2(a)]. Local increases of the zero-bias conductance are also seen in the raw data [Fig. 2(b)], and correlate well with the vortex positions determined by the best contrast. In order to remove the NSC, we delineate a small region in-between vortices, calculate the average spectrum in this region [inset of Fig. 2(b)], and

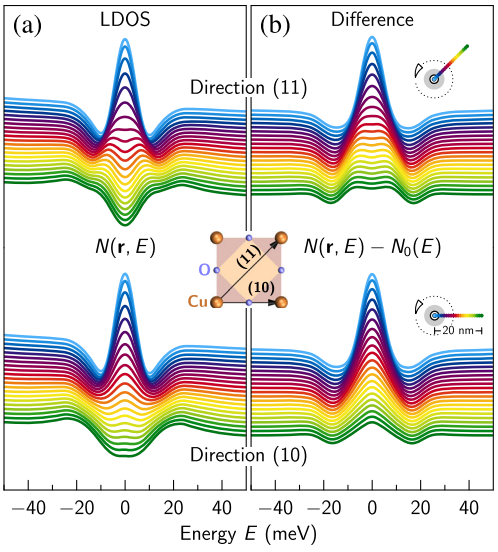

FIG. 1. (a) The self-consistent LDOS calculated in the BCS theory for an isolated vortex in a d-wave superconductor with Y123 band structure is shown along two paths starting at the vortex core (blue) and ending at two points 20 nm away from the core (green) along the nodal (11) and antinodal (10) directions. (b) Same data with the zero-field DOS subtracted from all curves. The vertical scale is arbitrary and the curves are shifted vertically for clarity. The insets show the CuO_2 unit cell with the two crystallographic directions, and representations of the vortex core (gray disks and arrows indicating the supercurrent direction) with the color-coded paths of the two spectral traces.

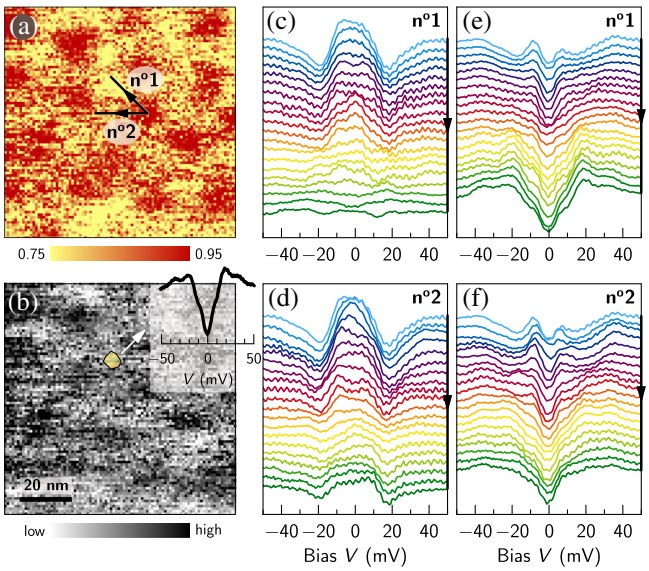

FIG. 2. (a) and (b) A 90×90 nm^2 area on the (001) surface of Y123 in a 6 T field, colored by (a) the ratio of the STS tunneling conductance at +5 and +17 mV, and (b) the conductance at zero bias. The inset in (b) shows the STS spectrum averaged over the small outlined region between vortices. Two series of difference spectra (raw STS data minus average spectrum shown in the inset) along the 20 nm paths indicated in (a) are displayed in (c) and (d). The color encodes distance from the core as in Fig. 1. Panels (e) and (f) show the raw dI/dV data along the two paths.

subtract this average from all spectra in the map. After subtraction, the spectral traces show the expected vortex signature with a maximum at zero bias in the cores. This is demonstrated in Figs. 2(c) and 2(d) with two traces running from one vortex core along the two directions shown in Fig. 2(a). The peak developing locally at zero bias after subtracting the same background from the spectra of each trace clearly shows there is a larger local density at low energy near the vortex cores. It is not an artifact of the subtraction. Similar results are found in all vortices.

A comparison of Figs. 2(c) and 2(d) with Fig. 1(b) reveals evident similarities, but also differences. Similarities include the zero-bias peak, which has its maximum at the core center and is suppressed with increasing distance from the center, the absence of superconducting coherence peaks in the core leading to symmetric dips at ± 17 meV in both experiment and theory, a striking spatial anisotropy, with the peak extending farther along path No. 2 than along path No. 1, reminiscent of the different decay lengths observed in the theory between directions 10 and 11. Among the differences, one notices the central peak being taller in Fig. 1(b) than in the measurements, and the spectrum appearing locally reinforced or split at intermediate distances along path No. 1 and No. 2, respectively, while Fig. 1(b) shows a monotonic evolution. We now demonstrate that these differences can be explained by considering that (i) the vortices are not isolated in the experiment, (ii) the relative orientation of the vortex and crystal lattices influences the LDOS, and (iii) the vortex lattice is disordered. Incorporating (i) in the theory reduces drastically the calculated peak height; (ii) means that the LDOS anisotropy depends upon the positions of nearby vortices; finally, (iii) implies that each vortex sits in a specific local environment and presents spectra different from its neighbors.

Figure 3 displays a series of spectral traces along various paths connecting either nearest-neighbor [Fig. 3(a)] or next-nearest neighbor [Fig. 3(b)] vortices. The notion of nearest- and next-nearest neighbor refers to a local fourfold coordination generally observed among the vortices, despite the long-range disorder in their arrangement. A trend is systematically observed: along a line connecting nearest-neighbor vortices, the zero-bias peak remains visible along the whole path, while it disappears along paths joining next-nearest neighbors. Considering the peak anisotropy as it is predicted by theory (Fig. 1), this trend suggests that the locally fourfold-coordinated vortex lattice tends to align along the crystalline axes, as we will confirm by a detailed modeling. In the absence of atomic resolution imaging, we infer the lattice orientation based on optical images of twin boundaries. Another lesson of Fig. 3 is that all vortices, although similar, are different: some show a single peak, others show a split peak; the height of these peaks is also varying. This variability reflects disorder in the vortex positions, resulting in irregular distributions of supercurrents around each core.

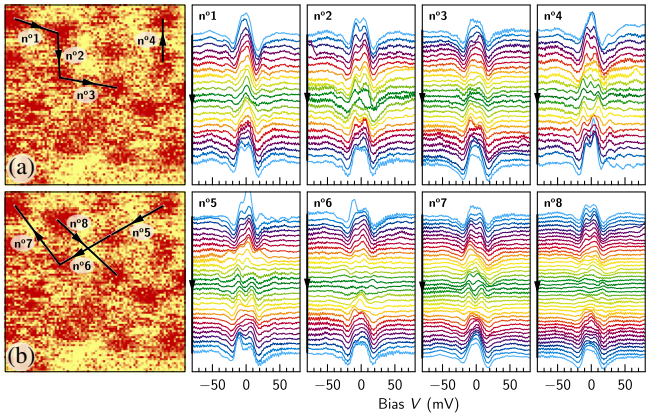

FIG. 3. Series of difference spectra [generated as in Figs. 2(c) and 2(d)] along several paths connecting (a) nearest-neighbor and (b) next-nearest-neighbor vortices. The spectra are shifted vertically and colored from blue (vortex center) to green (in-between two vortices).

We have undertaken large-scale simulations of the LDOS in disordered vortex configurations, in order to study how this modifies the core spectra with respect to the isolated vortex, and thus better understand the observations made by STS. Thanks to a new approach described in Ref. [53], we are able to compute the LDOS in a disordered vortex lattice with the same accuracy as in the isolated core. All relevant details are given as Supplemental Material [45], and we only briefly review here the key ingredients. The structure of the vortices in a finite field is deduced from the self-consistent solution in the ideal vortex lattice. We find that the LDOS changes dramatically with varying the orientation of the vortex lattice relative to the crystal axes. The system size required in order to compute the LDOS with our target resolution (3 meV) contains half a million unit cells and extends well beyond the area of our STS experiments, which contains roughly 54 500 Cu sites. Inside the STS field of view, we locate vortices at the positions indicated in Fig. 4(a). Outside, we generate vortex positions randomly, however, constraining the intervortex distance to be at least 16 nm. The resulting configurations show no orientational order, but short-range coordination similar to what is seen in the STS image. We do not imply that the actual vortex distribution outside the field of view has no orientational order—in fact, it probably has some [16]—but the available data prevent us from inferring such an order. We also vary the orientation of the crystal lattice with respect to the vortices. For each of 600 generated configurations, we calculate the LDOS along the paths No. 6 and No. 8 of Fig. 3 and compare with the experimental traces. With the configuration giving the smallest difference with experiment on these two traces, we recalculate the LDOS on the whole domain covered by STS with a resolution of 1 nm and deduce the theoretical map and traces shown Fig. 4(b).

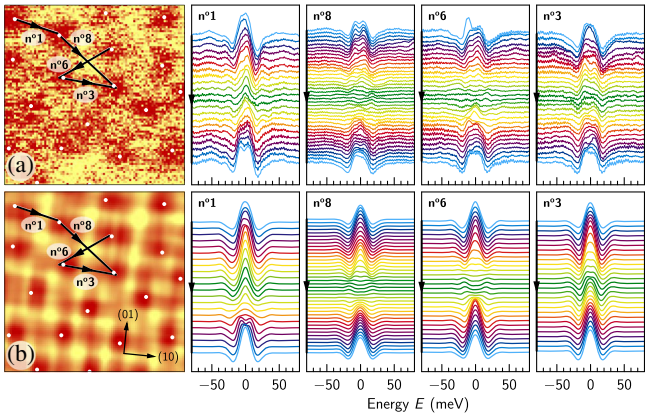

FIG. 4. (a) Same data as in Fig. 3 for traces joining nearest-neighbor (No. 1 and No. 3) and next-nearest-neighbor vortices (No. 6 and No. 8). (b) Calculated ratio $[N(\boldsymbol{r},5\,\mathrm{meV})+N_{\mathrm{NSC}}(5\,\mathrm{meV})]/[N(\boldsymbol{r},17\,\mathrm{meV})+N_{\mathrm{NSC}}(17\,\mathrm{meV})]$, where $N(\boldsymbol{r},E)$ is the theoretical LDOS and $N_{\mathrm{NSC}}(E)$ represents the non-superconducting background [45]. The simulated spectral traces are deduced from the theoretical LDOS by following the exact same procedure as applied to the experimental data. The white dots in (a) and (b) show the vortex positions, determined as the locations of maxima in (a) and corresponding to the phase singularity points of the order parameter in the simulation (b).

The simulation confirms that quasiparticle scattering off nearby vortices reduces the central peak in each vortex, that the LDOS is different in all cores, and that it depends on the configuration of the vortices outside the STS field of view. We also find that the agreement with experiment is systematically better if the orientation of the microscopic lattice is such that the traces No. 6 and No. 8 are close to a nodal direction, in agreement with the twin-boundary directions. Although our search for a good vortex configuration has focused on two traces connecting next-nearest neighbor vortices, the resulting model reproduces the difference between these traces and those connecting nearest-neighbor vortices. It is also striking that the model correctly predicts the contrast of the STS image and the apparent size of the vortex cores without any further adjustments. Figure 4(b) presents less spectral variations from core to core than Fig. 4(a), but this appears to be a compromise by which this configuration achieves the best overall agreement. Other vortex configurations that compete closely do show variations comparable with experiment, including split peaks in some of the vortices (Fig. S7 [45]). We emphasize that our procedure does not deliver the best fit, which would require us to optimize systematically the vortex positions rather than trying random configurations. The vortex positions *within* the field of view should be optimized as well. Figure 4(b) indeed reveals that the LDOS maxima are in general displaced with respect to the points where the order parameter vanishes: the LDOS gets polarized by asymmetries in the supercurrents [53,54]. Without any doubt, vortex configurations could be found that improve the agreement in Fig. 4, but we feel that such a costly optimization is unlikely to reveal new physics. Interestingly, the simulation presents vortex cores that appear to be split, e.g., at the beginning of path No. 6 (see also Fig. S8 [45]). Reference [55] reported a similar observation in Bi2212, which was ascribed to interaction with pinning centers. In Fig. 4(b) the splitting is merely a LDOS distortion due to an irregular distribution of the supercurrent.

In a clean BCS superconductor, the zero-temperature superfluid density n_{s0} equals the total electron density n [39]. Estimates based on the penetration depth show instead that $n_{s0}/n = 23\%$–34% in Y123 [56]. The analysis of STS data yields similar relations between the SC and NSC, with some model dependence, 14% in Ref. [18], 25% in the present work [45]. In a one-channel picture, the property $n_{s0} \ll n$ requires large pairing fluctuations that would invalidate a mean-field description. Our results show that the mean-field theory works well in vortices, though. Another possibility would be that superconductivity emerges in a population of low-energy quasiparticles carrying only a small fraction of the spectral weight: in the RVB theory, the quasiparticle weight behaves as $2x/(1+x)$ as a function of doping x [59], as observed in optical data of underdoped cuprates [60], which yields a value close to 25% at optimal doping. In this scenario, the NSC should disappear with overdoping and the vortices should present a clear zero-bias peak, a challenge for future STS experiments. Alternatively, one can imagine two-channel scenarios. It has been recently proposed that the cuprate superconductivity is lead by oxygen $2p$ rather than copper $3d$ holes [61]. We speculate that the copper holes remain localized and form the NSC (in the specific case of Y123, where the zero-bias conductance is large, we cannot rule out a parasitic surface channel as another contribution to the NSC), while the oxygen holes are responsible for the recently uncovered universal Fermi-liquid signatures [62] and enter the SC condensate. While the origin of pairing in this condensate remains mysterious, its spectroscopic properties are well described by the BCS theory, as we have demonstrated by unveiling the Caroli–de Gennes–Matricon-like states in the vortex cores.

We thank T. Giamarchi and D. van der Marel for their comments on the manuscript, N. Hussey and G. Deutscher for discussions, and G. Manfrini and A. Guipet for their technical assistance. This research was supported by the Swiss National Science Foundation under Division II. The calculations were performed in the University of Geneva with the clusters Mafalda and Baobab.

*christoph.renner@unige.ch

[1] C. Caroli, P. G. de Gennes, and J. Matricon, Bound Fermion States on a Vortex Line in a Type II Superconductor, Phys. Lett. **9**, 307 (1964).

[2] H. F. Hess, R. B. Robinson, R. C. Dynes, J. M. Valles, and J. V. Waszczak, Scanning-Tunneling-Microscope Observation of the Abrikosov Flux Lattice and the Density of States near and inside a Fluxoid, Phys. Rev. Lett. **62**, 214 (1989).

[3] C. Renner, A. D. Kent, P. Niedermann, Ø. Fischer, and F. Lévy, Scanning Tunneling Spectroscopy of a Vortex Core from the Clean to the Dirty Limit, Phys. Rev. Lett. **67**, 1650 (1991).

[4] H. Suderow, I. Guillamón, J. G. Rodrigo, and S. Vieira, Imaging superconducting vortex cores and lattices with a scanning tunneling microscope, Supercond. Sci. Technol. **27**, 063001 (2014).

[5] Y. DeWilde, M. Iavarone, U. Welp, V. Metlushko, A. E. Koshelev, I. Aranson, G. W. Crabtree, and P. C. Canfield, Scanning Tunneling Microscopy Observation of a Square Abrikosov Lattice in $LuNi_2B_2C$, Phys. Rev. Lett. **78**, 4273 (1997).

[6] M. R. Eskildsen, M. Kugler, S. Tanaka, J. Jun, S. M. Kazakov, J. Karpinski, and Ø. Fischer, Vortex Imaging in the π Band of Magnesium Diboride, Phys. Rev. Lett. **89**, 187003 (2002).

[7] H. Nishimori, K. Uchiyama, S.-i. Kaneko, A. Tokura, H. Takeya, K. Hirata, and N. Nishida, First observation of the fourfold-symmetric and quantum regime vortex core in YNi_2B_2C by scanning tunneling microscopy and spectroscopy, J. Phys. Soc. Jpn. **73**, 3247 (2004).

[8] I. Guillamón, H. Suderow, S. Vieira, L. Cario, P. Diener, and P. Rodière, Superconducting Density of States and Vortex Cores of 2H-NbS_2, Phys. Rev. Lett. **101**, 166407 (2008).

[9] B. B. Zhou, S. Misra, E. H. da Silva Neto, P. Aynajian, R. E. Baumbach, J. D. Thompson, E. D. Bauer, and A. Yazdani, Visualizing nodal heavy fermion superconductivity in $CeCoIn_5$, Nat. Phys. **9**, 474 (2013).

[10] Z. Du, D. Fang, Z. Wang, Y. Li, G. Du, H. Yang, X. Zhu, and H.-H. Wen, Anisotropic superconducting gap and elongated vortices with Caroli–De Gennes–Matricon states in the new superconductor $Ta_4Pd_3Te_{16}$, Sci. Rep. **5**, 9408 (2015).

[11] Y. Yin, M. Zech, T. L. Williams, X. F. Wang, G. Wu, X. H. Chen, and J. E. Hoffman, Scanning Tunneling Spectroscopy and Vortex Imaging in the Iron Pnictide Superconductor $BaFe_{1.8}Co_{0.2}As_2$, Phys. Rev. Lett. **102**, 097002 (2009).

[12] L. Shan, Y.-L. Wang, B. Shen, B. Zeng, Y. Huang, A. Li, D. Wang, H. Yang, C. Ren, Q.-H. Wang, S. H. Pan, and H.-H. Wen, Observation of ordered vortices with Andreev bound states in $Ba_{0.6}K_{0.4}Fe_2As_2$, Nat. Phys. **7**, 325 (2011).

[13] C.-L. Song, Y.-L. Wang, P. Cheng, Y.-P. Jiang, W. Li, T. Zhang, Z. Li, K. He, L. Wang, J.-F. Jia, H.-H. Hung, C. Wu, X. Ma, X. Chen, and Q.-K. Xue, Direct observation of nodes and twofold symmetry in FeSe superconductor, Science **332**, 1410 (2011).

[14] T. Hanaguri, K. Kitagawa, K. Matsubayashi, Y. Mazaki, Y. Uwatoko, and H. Takagi, Scanning tunneling microscopy/spectroscopy of vortices in LiFeAs, Phys. Rev. B **85**, 214505 (2012).

[15] Q. Fan, W. H. Zhang, X. Liu, Y. J. Yan, M. Q. Ren, R. Peng, H. C. Xu, B. P. Xie, J. P. Hu, T. Zhang, and D. L. Feng, Plain s-wave superconductivity in single-layer FeSe on $SrTiO_3$ probed by scanning tunnelling microscopy, Nat. Phys. **11**, 946 (2015).

[16] I. Maggio-Aprile, C. Renner, A. Erb, E. Walker, and Ø. Fischer, Direct Vortex Lattice Imaging and Tunneling Spectroscopy of Flux Lines on $YBa_2Cu_3O_{7-\delta}$, Phys. Rev. Lett. **75**, 2754 (1995).

[17] K. Shibata, M. Maki, T. Nishizaki, and N. Kobayashi, Scanning tunneling spectroscopy studies on vortices in $YBa_2Cu_3O_y$ single crystals, Physica (Amsterdam) **392C–396C**, 323 (2003); K. Shibata, T. Nishizaki, M. Maki, and N. Kobayashi, Local spectroscopy and vortex-core imaging on chemically wet-etched surfaces of $YBa_2Cu_3O_y$ by scanning tunneling microscopy/spectroscopy, Supercond. Sci. Technol. **23**, 085004 (2010).

[18] J. Bruér, I. Maggio-Aprile, N. Jenkins, Z. Ristić, A. Erb, C. Berthod, Ø. Fischer, and C. Renner, Revisiting the vortex-core tunnelling spectroscopy in $YBa_2Cu_3O_{7-\delta}$, Nat. Commun. **7**, 11139 (2016).

[19] C. Renner, B. Revaz, K. Kadowaki, I. Maggio-Aprile, and Ø. Fischer, Observation of the Low Temperature Pseudogap in the Vortex Cores of $Bi_2Sr_2CaCu_2O_{8+\delta}$, Phys. Rev. Lett. **80**, 3606 (1998).

[20] B. W. Hoogenboom, C. Renner, B. Revaz, I. Maggio-Aprile, and Ø. Fischer, Low-energy structures in vortex core tunneling spectra in $Bi_2Sr_2CaCu_2O_{8+\delta}$, Physica (Amsterdam) **332C**, 440 (2000).

[21] S. H. Pan, E. W. Hudson, A. K. Gupta, K.-W. Ng, H. Eisaki, S. Uchida, and J. C. Davis, STM Studies of the Electronic Structure of Vortex Cores in $Bi_2Sr_2CaCu_2O_{8+\delta}$, Phys. Rev. Lett. **85**, 1536 (2000).

[22] K. Matsuba, H. Sakata, N. Kosugi, H. Nishimori, and N. Nishida, Ordered vortex lattice and intrinsic vortex core states in $Bi_2Sr_2CaCu_2O_x$ studied by scanning tunneling microscopy and spectroscopy, J. Phys. Soc. Jpn. **72**, 2153 (2003); K. Matsuba, S. Yoshizawa, Y. Mochizuki, T. Mochiku, K. Hirata, and N. Nishida, Anti-phase modulation of electron- and hole-like states in vortex core of $Bi_2Sr_2CaCu_2O_x$ probed by scanning tunneling spectroscopy, J. Phys. Soc. Jpn. **76**, 063704 (2007).

[23] G. Levy, M. Kugler, A. A. Manuel, Ø. Fischer, and M. Li, Fourfold Structure of Vortex-Core States in $Bi_2Sr_2CaCu_2O_{8+\delta}$, Phys. Rev. Lett. **95**, 257005 (2005).

[24] S. Yoshizawa, T. Koseki, K. Matsuba, T. Mochiku, K. Hirata, and N. Nishida, High-resolution scanning tunneling spectroscopy of vortex cores in inhomogeneous electronic states of $Bi_2Sr_2CaCu_2O_x$, J. Phys. Soc. Jpn. **82**, 083706 (2013).

[25] Y. Wang and A. H. MacDonald, Mixed-state quasiparticle spectrum for d-wave superconductors, Phys. Rev. B **52**, R3876 (1995).

[26] M. Franz and Z. Tešanović, Self-Consistent Electronic Structure of a $d_{x^2-y^2}$ and a $d_{x^2-y^2}+id_{xy}$ Vortex, Phys. Rev. Lett. **80**, 4763 (1998).

[27] C. Berthod, Bogoliubov quasiparticles coupled to the antiferromagnetic spin mode in a vortex core, Phys. Rev. B **92**, 214505 (2015).

[28] D. P. Arovas, A. J. Berlinsky, C. Kallin, and S.-C. Zhang, Superconducting Vortex with Antiferromagnetic Core, Phys. Rev. Lett. **79**, 2871 (1997).

[29] A. Himeda, M. Ogata, Y. Tanaka, and S. Kashiwaya, Theory of the quasiparticle spectra around a vortex in the two-dimensional t-J model, J. Phys. Soc. Jpn. **66**, 3367 (1997).

[30] B. M. Andersen, H. Bruus, and P. Hedegård, SO(5) theory of insulating vortex cores in high-T_c materials, Phys. Rev. B **61**, 6298 (2000).

[31] J.-i. Kishine, P. A. Lee, and X.-G. Wen, Staggered Local Density-of-States around the Vortex in Underdoped Cuprates, Phys. Rev. Lett. **86**, 5365 (2001).

[32] C. Berthod and B. Giovannini, Density of States in High-T_c Superconductor Vortices, Phys. Rev. Lett. **87**, 277002 (2001).

[33] J.-X. Zhu and C. S. Ting, Quasiparticle States at a d-Wave Vortex Core in High-T_c Superconductors: Induction of Local Spin Density Wave Order, Phys. Rev. Lett. **87**, 147002 (2001).

[34] M. M. Maśka and M. Mierzejewski, Vortex structure in d-density wave scenario, Phys. Rev. B **68**, 024513 (2003).

[35] M. Fogelström, Structure of the core of magnetic vortices in d-wave superconductors with a subdominant triplet pairing mechanism, Phys. Rev. B **84**, 064530 (2011).

[36] F. C. Zhang and T. M. Rice, Effective Hamiltonian for the superconducting Cu oxides, Phys. Rev. B **37**, 3759 (1988).

[37] V. J. Emery, Theory of High-T_c Superconductivity in Oxides, Phys. Rev. Lett. **58**, 2794 (1987).

[38] Ø. Fischer, M. Kugler, I. Maggio-Aprile, C. Berthod, and C. Renner, Scanning tunneling spectroscopy of high-temperature superconductors, Rev. Mod. Phys. **79**, 353 (2007).

[39] A. J. Leggett, On the superfluid fraction of an arbitrary many-body system at $T = 0$, J. Stat. Phys. **93**, 927 (1998).

[40] Y. J. Uemura *et al.*, Universal Correlations between T_c and n_s/m^* (Carrier Density over Effective Mass) in High-T_c Cuprate Superconductors, Phys. Rev. Lett. **62**, 2317 (1989).

[41] C. Bernhard, C. Niedermayer, U. Binninger, A. Hofer, C. Wenger, J. L. Tallon, G. V. M. Williams, E. J. Ansaldo, J. I. Budnick, C. E. Stronach, D. R. Noakes, and M. A. Blankson-Mills, Magnetic penetration depth and condensate density of cuprate high-T_c superconductors determined by muon-spin-rotation experiments, Phys. Rev. B **52**, 10488 (1995).

[42] I. Božović, X. He, J. Wu, and A. T. Bollinger, Dependence of the critical temperature in overdoped copper oxides on superfluid density, Nature (London) **536**, 309 (2016).

[43] A. Junod, A. Erb, and C. Renner, Specific heat of high temperature superconductors in high fields at T_c: From BCS to Bose-Einstein condensation, Physica (Amsterdam) **317C–318C**, 333 (1999).

[44] J. E. Hoffman, E. W. Hudson, K. M. Lang, V. Madhavan, H. Eisaki, S. Uchida, and J. C. Davis, A four unit cell periodic pattern of quasi-particle states surrounding vortex cores in $Bi_2Sr_2CaCu_2O_{8+\delta}$, Science **295**, 466 (2002).

[45] See Supplemental Material at http://link.aps.org/supplemental/10.1103/PhysRevLett.119.237001 for a presentation of the model and calculation methods, which includes Refs. [46–51].

[46] J. D. Jorgensen, B. W. Veal, A. P. Paulikas, L. J. Nowicki, G. W. Crabtree, H. Claus, and W. K. Kwok, Structural properties of oxygen-deficient $YBa_2Cu_3O_{7-\delta}$, Phys. Rev. B **41**, 1863 (1990).

[47] W. A. Atkinson, The effect of CuO chains on the local density of states in the vortex phase of $YBa_2Cu_3O_7$, Supercond. Sci. Technol. **22**, 014005 (2009).

[48] M. C. Schabel, C.-H. Park, A. Matsuura, Z.-X. Shen, D. A. Bonn, R. Liang, and W. N. Hardy, Angle-resolved photoemission on untwinned $YBa_2Cu_3O_{6.95}$. I. Electronic structure and dispersion relations of surface and bulk bands, Phys. Rev. B **57**, 6090 (1998); Angle-resolved photoemission on untwinned $YBa_2Cu_3O_{6.95}$. II. Determination of Fermi surfaces, Phys. Rev. B **57**, 6107 (1998).

[49] M. Ichioka, N. Hayashi, N. Enomoto, and K. Machida, Vortex structure in d-wave superconductors, Phys. Rev. B **53**, 15316 (1996).

[50] S. Torquato and F. H. Stillinger, Local density fluctuations, hyperuniformity, and order metrics, Phys. Rev. E **68**, 041113 (2003).

[51] A. Weismann, M. Wenderoth, S. Lounis, P. Zahn, N. Quaas, R. G. Ulbrich, P. H. Dederichs, and S. Blügel, Seeing the Fermi surface in real space by nanoscale electron focusing, Science **323**, 1190 (2009).

[52] B. M. Uranga, M. N. Gastiasoro, and B. M. Andersen, Electronic vortex structure of Fe-based superconductors: Application to LiFeAs, Phys. Rev. B **93**, 224503 (2016).

[53] C. Berthod, Vortex spectroscopy in the vortex glass: A real-space numerical approach, Phys. Rev. B **94**, 184510 (2016).

[54] C. Berthod, Quasiparticle spectra of Abrikosov vortices in a uniform supercurrent flow, Phys. Rev. B **88**, 134515 (2013).

[55] B. W. Hoogenboom, M. Kugler, B. Revaz, I. Maggio-Aprile, Ø. Fischer, and C. Renner, Shape and motion of vortex cores in $Bi_2Sr_2CaCu_2O_{8+\delta}$, Phys. Rev. B **62**, 9179 (2000).

[56] At an optimal hole doping of 0.16, the nominal carrier density of the bilayer Y123 is $n = 2 \times 0.84/(abc) = 9.7\ \mathrm{nm}^{-3}$ with the unit-cell parameters $(a, b, c) = (3.82, 3.89, 11.68)$ Å. With an effective mass of typically 2–3 times the electron mass [57] and a zero-temperature penetration depth $\lambda = 1600$ Å [58], the estimated superfluid density $n_s = m^*/(\mu_0 e^2 \lambda^2)$ is 2.2–3.3 nm^{-3}.

[57] W. J. Padilla, Y. S. Lee, M. Dumm, G. Blumberg, S. Ono, K. Segawa, S. Komiya, Y. Ando, and D. N. Basov, Constant effective mass across the phase diagram of high-T_c cuprates, Phys. Rev. B **72**, 060511 (2005).

[58] D. N. Basov, R. Liang, D. A. Bonn, W. N. Hardy, B. Dabrowski, M. Quijada, D. B. Tanner, J. P. Rice, D. M. Ginsberg, and T. Timusk, In-Plane Anisotropy of the Penetration Depth in $YBa_2Cu_3O_{7-x}$ and $YBa_2Cu_4O_8$ Superconductors, Phys. Rev. Lett. **74**, 598 (1995).

[59] P. W. Anderson, P. A. Lee, M. Randeria, T. M. Rice, N. Trivedi, and F. C. Zhang, The physics behind high-temperature superconducting cuprates: the 'plain vanilla' version of RVB, J. Phys. Condens. Matter **16**, R755 (2004).

[60] S. I. Mirzaei, D. Stricker, J. N. Hancock, C. Berthod, A. Georges, E. van Heumen, M. K. Chan, X. Zhao, Y. Li, M. Greven, N. Barišić, and D. van der Marel, Spectroscopic

evidence for Fermi liquid-like energy and temperature dependence of the relaxation rate in the pseudogap phase of the cuprates, Proc. Natl. Acad. Sci. U.S.A. **110**, 5774 (2013).

[61] D. Rybicki, M. Jurkutat, S. Reichardt, C. Kapusta, and J. Haase, Perspective on the phase diagram of cuprate high-temperature superconductors, Nat. Commun. **7**, 11413 (2016).

[62] N. Barišić, M. K. Chan, Y. Li, G. Yu, X. Zhao, M. Dressel, A. Smontara, and M. Greven, Universal sheet resistance and revised phase diagram of the cuprate high-temperature superconductors, Proc. Natl. Acad. Sci. U.S.A. **110**, 12235 (2013).